



# Portable electronic nose based on carbon nanotube-SnO<sub>2</sub> gas sensors and its application for detection of methanol contamination in whiskeys

Chatchawal Wongchoosuk<sup>a</sup>, Anurat Wisitsoraat<sup>b</sup>, Adisorn Tuantranont<sup>b</sup>, Teerakiat Kerdcharoen<sup>a,c,\*</sup>

<sup>a</sup> Department of Physics and Center of Nanoscience and Nanotechnology, Faculty of Science, Mahidol University, Bangkok 10400, Thailand

<sup>b</sup> Nanoelectronic and MEMS Lab, National Electronic and Computer Technology Center, Pathumthani 12120, Thailand

<sup>c</sup> NANOTEC Center of Excellence at Mahidol University, National Nanotechnology Center, Thailand

## ARTICLE INFO

### Article history:

Received 11 March 2009

Received in revised form 16 March 2010

Accepted 24 March 2010

Available online 31 March 2010

### Keywords:

E-nose

Carbon nanotube

Metal oxide

Gas sensor

Feature extraction techniques

## ABSTRACT

In this paper, a portable electronic nose (E-nose) based on hybrid carbon nanotube-SnO<sub>2</sub> gas sensors is described. The hybrid gas sensors were fabricated using electron beam (E-beam) evaporation by means of powder mixing. The instrument employs feature extraction techniques including integral and primary derivative, which lead to higher classification performance as compared to the classical features ( $\Delta R$  and  $\Delta R/R_0$ ). It was shown that doping of carbon nanotube (CNT) improves the sensitivity of hybrid gas sensors, while quantity of CNT has a direct effect on the selectivity to volatile organic compounds, i.e., methanol (MeOH) and ethanol (EtOH). The real-world applications of this E-nose were also demonstrated. Based on the proposed methods, this instrument can monitor and classify 1 vol% of MeOH contamination in whiskeys.

© 2010 Elsevier B.V. All rights reserved.

## 1. Introduction

Nowadays, electronic nose (E-nose) has become a powerful tool to evaluate the aroma compounds during the quality control process of foods and beverages [1–3]. Besides, E-noses have also been employed for public safety [4], environment protection [5,6], disease diagnostics [7], etc. E-nose is composed of an array of gas sensors made from various materials that display distinct gas-sensing behaviors of which differentiation can be combined and interpreted via pattern recognition techniques [8]. Among the available sensing materials, metal oxide semiconductors (MOS), such as SnO<sub>2</sub> and WO<sub>3</sub>, have been the most popular due to their high sensitivity to a rich set of volatile compounds.

Doping has long been used as a traditional mean to obtain new MOS gas sensors that exhibit gas-sensing properties differentiated from the original ones. Recently, much interest has been focused on carbon nanotube (CNT) as potential dopant, due to its special electronic properties and high specific surface area that can boost catalytic reactions occurring at the metal oxide surface. The hybrid CNT-SnO<sub>2</sub> gas sensors prepared by different techniques have been reported to have excellent responses to NO<sub>2</sub> [9,10], CO [10], NH<sub>3</sub>

[11], H<sub>2</sub> [12], CHOH [13] and indoor air pollutants [14]. Among such techniques, co-evaporation of SnO<sub>2</sub>/CNT is a relatively new concept to form hybrid CNT-SnO<sub>2</sub> gas sensors [15,16]. It offers extensive possibilities for controlling the film structure and morphology with high deposition rates, low contamination, high reliability and high productivity. However, there have been very few reports on CNT-SnO<sub>2</sub> gas sensors prepared by this technique, and this sensor system has not been applied for E-nose applications.

In this work, we report on an E-nose based on hybridized CNT-SnO<sub>2</sub> gas sensors prepared by electron beam (E-beam) evaporation, which is inexpensive, fast, portable, reliable and suitable for use for the detection and classification of both solid and liquid samples. In addition, feature extraction techniques including integral and primary derivative are proposed for improving classification performance by principal component analysis (PCA). This E-nose was tested in a real-world application, i.e., for detecting methanol (MeOH) contaminant in whiskeys. This system will be a useful tool for quality assurance of whiskey produced by village industries.

## 2. Experimental

### 2.1. Fabrication of gas sensors

The gas sensors were fabricated by E-beam evaporation. Top and cross-sectional views of sensor structure are shown in Fig. 1a and b, respectively. First, Cr/Au interdigitated electrodes on alumina substrates were prepared. Prior to deposition of the electrodes,

\* Corresponding author at: Department of Physics and Center of Nanoscience and Nanotechnology, Faculty of Science, Mahidol University, Bangkok 10400, Thailand. Tel.: +66 866037395; fax: +66 22015843.

E-mail address: [sctkc@mahidol.ac.th](mailto:sctkc@mahidol.ac.th) (T. Kerdcharoen).

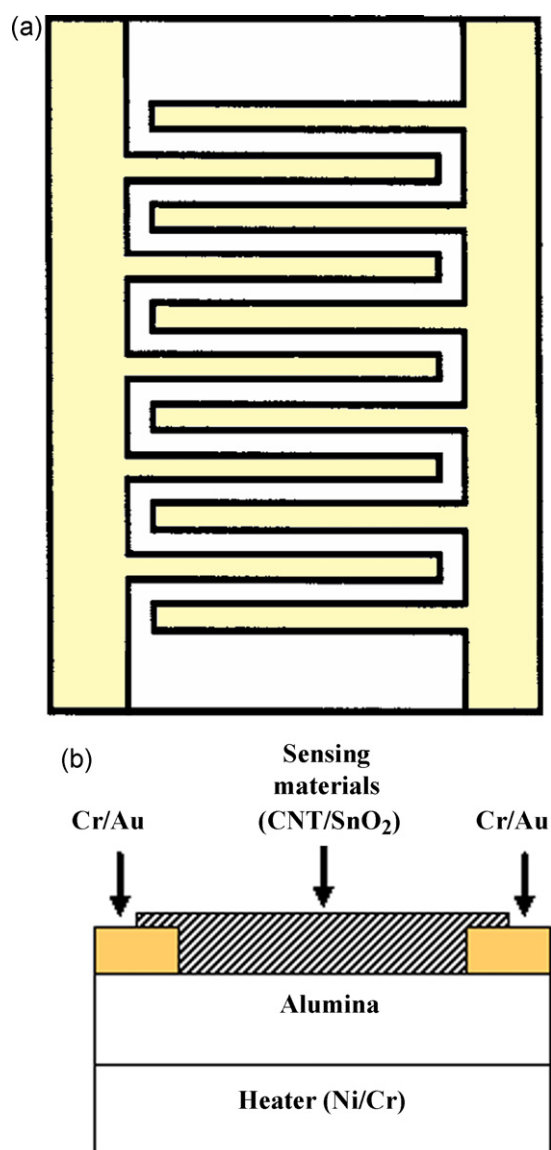


**Fig. 1.** Structure of the gas sensor; (a) top view of interdigitated electrode, (b) cross-sectional view.

the substrates were cleaned by oxygen-ion bombardment under a vacuum pressure of  $\sim 10^{-4}$  Torr in order to improve the adhesion of the film to the substrates. Cr and Au layers were then successively E-beam evaporated over the alumina substrates through electroplated-Ni shadow masks. These shadow masks were fabricated by means of standard photolithography and electroplating of Ni. The masks were employed by attaching them to the substrates using strong magnets. The resulted thickness of Cr and Au layers were  $\sim 50$  nm and  $\sim 200$  nm, respectively. The width, spacing, and length of the interdigitated electrodes are approximately  $100 \mu\text{m}$ ,  $100 \mu\text{m}$ , and  $1$  mm, respectively.

Multi-walled CNT powder was synthesized by thermal chemical vapor deposition (CVD) in a lab-made horizontal tube furnace. Iron catalyst powder was loaded in the tube furnace and heated up until the growth temperature of  $700^\circ\text{C}$  was reached. The system was then maintained under the hydrogen gas flow of  $1.5$  l/min at the atmospheric pressure. Next, acetylene gas was introduced into the system for  $2$  h for CNT synthesis. The flow ratio between acetylene and hydrogen was approximately  $1:4$ . The remaining catalysts were removed from CNTs by chemical oxidation in  $4$  M nitric acid at room temperature for  $4$  h. Then, CNTs were rinsed with DI

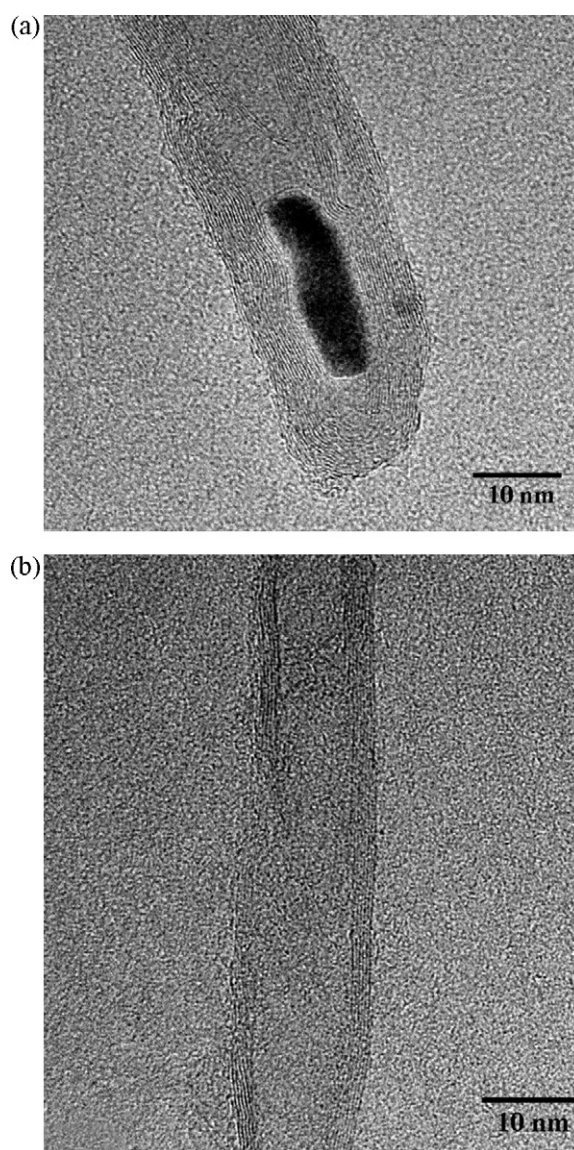


**Fig. 2.** Typical TEM images of multi-walled CNT (a) before and (b) after purification.

water and dehydrated at  $150^\circ\text{C}$  for  $2$  h [17]. Transmission electron microscope (TEM) images of the CNT before and after chemical oxidation treatments are shown in Fig. 2a and b, respectively. It is evident that the iron catalysts were effectively removed and the number of CNT walls was reduced. CNT–SnO<sub>2</sub> mixed powders were prepared with  $0.5$  wt% and  $1$  wt% concentrations by mixing  $15$  g of SnO<sub>2</sub> powder with  $0.075$  g and  $0.15$  g of CNT powders, respectively. The mixed powders were thoroughly mixed by grinding in a mortar for  $30$  min. The pure SnO<sub>2</sub> and mixed powders were compressed into cylindrical pellets in a hard steel mold by a hydraulic compressor at a pressure of  $15$  tons. Next, the compressed SnO<sub>2</sub> and mixed CNT–SnO<sub>2</sub> materials ( $0.5$  wt% and  $1$  wt% CNTs) were loaded in E-beam chamber and evaporated over the interdigitated electrodes through an electroplated shadow mask with square window pattern that aligned to the interdigitated area at an operating vacuum of  $\sim 10^{-5}$  Torr. The evaporation condition was based on the previous studies by Wisitsoraat et al. [15,16]. The film thickness of sensing materials is  $\sim 300$  nm as measured *in situ* by quartz crystal monitor. The evaporated film was then annealed at  $500^\circ\text{C}$  for  $3$  h. Finally, a NiCr (Ni  $80\%$  and Cr  $20\%$ ) layer was also E-beam evaporated over the backside of substrate to perform as a heating unit. The NiCr heater

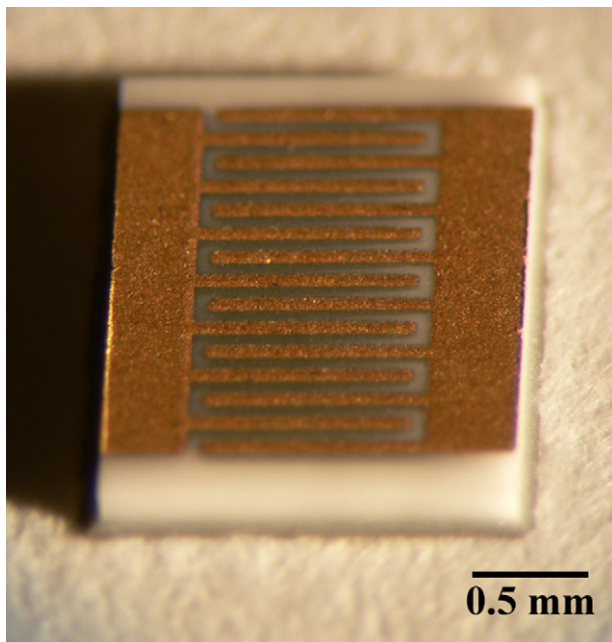


Fig. 3. Photograph of the fabricated sensor.

can perform heating up to 350 °C. A photograph of fabricated sensor is shown in Fig. 3.

## 2.2. Portable E-nose system

An E-nose has been developed in a briefcase form factor (19.5 cm × 29.5 cm × 10 cm). Fig. 4 shows a schematic diagram indicating the key components of the portable E-nose system. The clean air produced from a pump carries aroma molecules of sample into a sensor chamber at flow rate 2 l/min. Four electrical solenoid valves

were used to avoid mixing of gas from the reference and the sample. It is necessary for this type of measurement to switch between a reference and a sample glass in order to reduce the humidity effects [18,19].

The sensor array consisting of three gas sensors: SnO<sub>2</sub>, 0.5 wt% CNT–SnO<sub>2</sub> and 1 wt% CNT–SnO<sub>2</sub> was symmetrically embedded at the bottom of a Teflon chamber. A simple linear circuit, called as voltage divider, was employed for measuring the resistance of each gas sensor. The load resistance is 20 kΩ ± 1% while the resistance of each gas sensor lies within the range 20–40 kΩ. The voltage input is fixed at 5 V. The data were collected every second by a notebook computer using a data acquisition card (NI-DAQ 6008) under LabVIEW software for subsequent analyses.

## 2.3. PCA and feature extraction techniques

PCA was used for pattern recognition and classification of samples measured by the portable E-nose. PCA is a statistical technique that allows an easy visualization of all correlated information [20]. In principles, PCA process contains five steps as follows:

- i. Get data from matrix,  $X_{M \times N}$ . The row  $M$  represents different repetition of the experiment and the column  $N$  represents the number of independent sensors.
- ii. Normalize the data matrix,  $Norm(X_{M \times N})$ , by the mean subtraction. The mean of each  $N$  column is calculated and subtracted from the data set. Hence, the new data set produces the mean equal to zero.
- iii. Calculate the covariance matrix,  $Cov(X_{M \times N})$ , and calculate eigenvectors and eigenvalues of the covariance matrix. The calculated eigenvectors must be unit eigenvectors.
- iv. Rearrange the eigenvectors and eigenvalues. The eigenvectors are ordered by eigenvalues from highest to lowest,  $(Cov(X_{M \times N}))_{max \rightarrow min}$ .

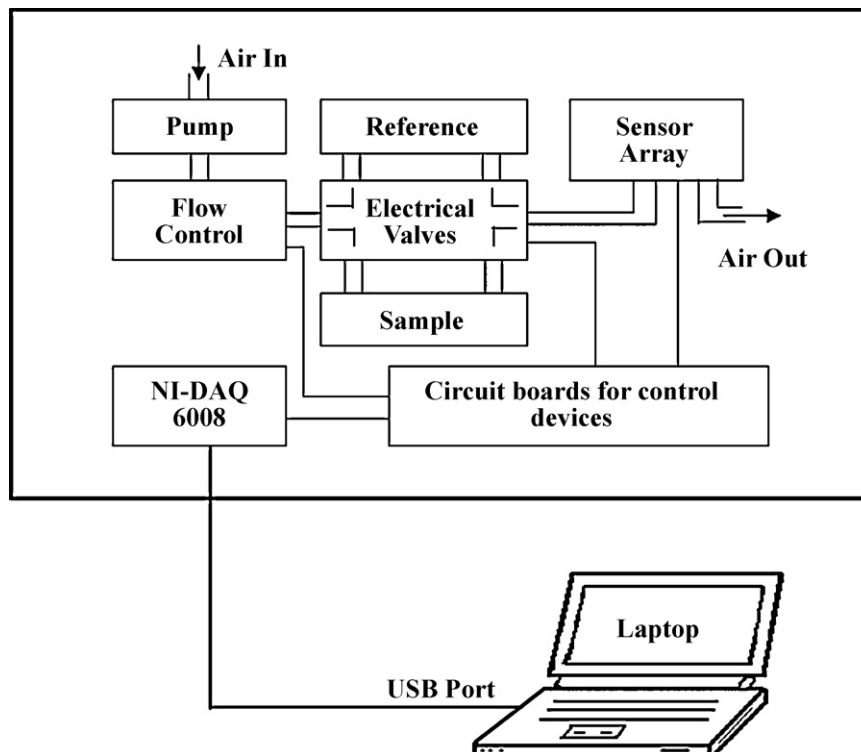
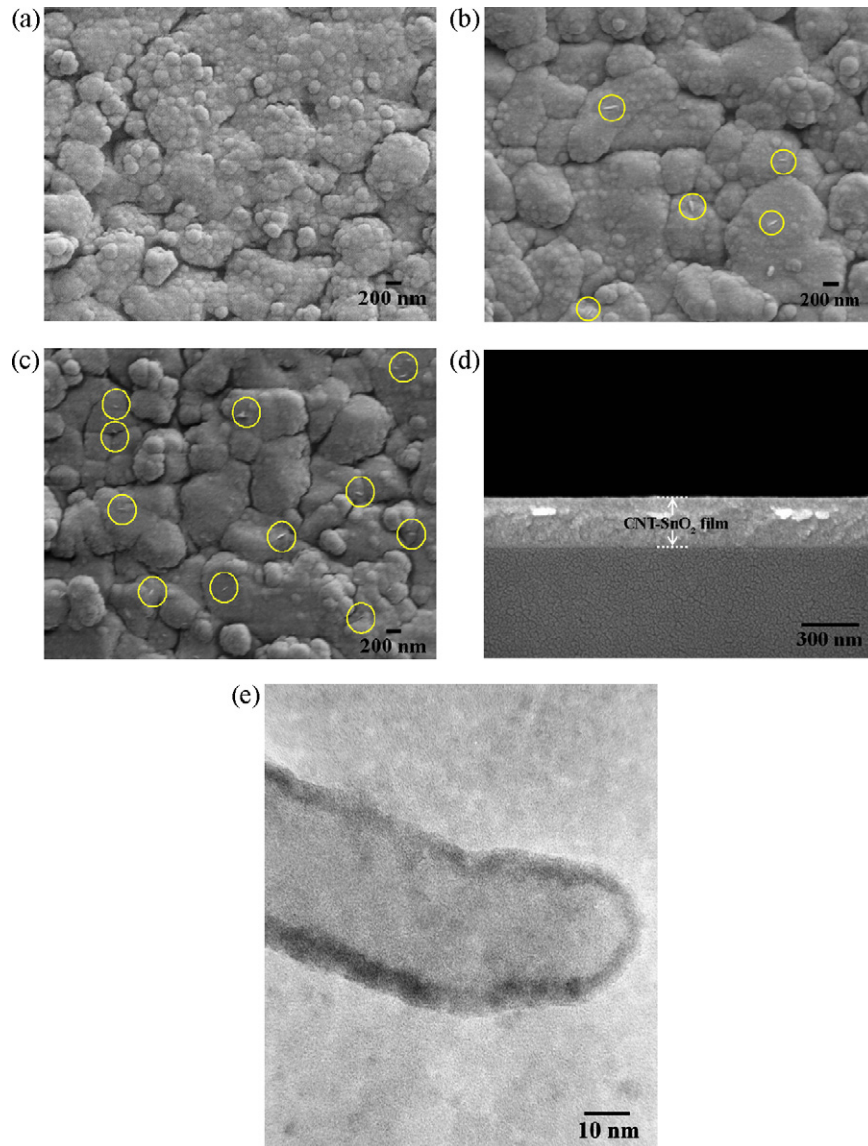


Fig. 4. Schematic diagram of the portable E-nose system.



**Fig. 5.** SEM images of sensing films; (a) undoped SnO<sub>2</sub> film, (b) 0.5 wt% CNT-SnO<sub>2</sub> film and (c) 1 wt% CNT-SnO<sub>2</sub> film. The yellow circles in (b) and (c) indicate CNT fragments, (d) typical cross-sectional SEM image of CNT-SnO<sub>2</sub> film and (e) typical HRTEM image of CNT-SnO<sub>2</sub> film.

v. Obtain the PCA result by matrix multiplication and transpose,  $((\overrightarrow{Cov}(X_{M \times N}))_{\max \rightarrow \min} \otimes Norm(X_{M \times N}))^T$ . The obtained new data set with orthogonal linear transformation has been plotted in two or three dimensions containing the most relevant of the data set.

However, preprocessing or feature extraction from the acquired sensor signal prior to the use of PCA is very necessary to get better separation. Two features: integral and primary derivative, having specific physical meanings were proposed as the following formulation:

$$\text{Integral : } I_t = \int_a^b V_{out} dt \quad (1)$$

$$\text{Primary derivative : } D_t = \frac{dV_{out}}{dt} \quad (2)$$

where  $V_{out}$  represents a sensor signal.

In real calculation, the integral and primary derivative of  $V_{out}$  are obtained from the elements of  $y_i^I$  and  $y_i^D$ , respectively, using the

following relations:

$$y_i^I = \frac{1}{6} \sum_{j=0}^i (x_{j-1} + 4x_j + x_{j+1}) dt \quad (3)$$

$$y_i^D = \frac{1}{2dt} (x_{i+1} - x_{i-1}) \quad (4)$$

where  $i = 0, 1, 2, \dots, n-1$  and  $n$  is the number of samples.

In addition, signal integral refers to the accumulative total of the reaction degree-changing while primary derivative of signal represents the reaction rate [21,22].

### 3. Results and discussion

#### 3.1. Characterization of gas-sensing films

Fig. 5a–c illustrates morphology of the sensing films by scanning electron microscopy (SEM), showing the presence of metal oxide grains. Spherical SnO<sub>2</sub> particles are clearly observed in the undoped tin oxide film (see Fig. 5a). In the CNT-doped SnO<sub>2</sub> films, such spherical particles are smoothed out and smaller SnO<sub>2</sub> grain

sizes are observed. In addition, the CNTs are well embedded and randomly arranged inside the  $\text{SnO}_2$  film as circled in Fig. 5b and c. It can be seen that although the distributions of CNTs in the films are quite random, the densities of the observed CNTs are proportional to the concentration of CNTs in the initial mixed powders. Therefore, the amount of CNTs in the film can be well controlled by varying the percentage of CNTs in the initial mixed powder.

Typical cross-sectional SEM image of CNT-doped  $\text{SnO}_2$  film is shown in Fig. 5d. It indicates that the film thickness is about 270 nm, slightly lower than the expected value of 300 nm. The small discrepancy should be due to some calibration inaccuracies of quartz crystal monitor. The detailed structure of CNT– $\text{SnO}_2$  composite was characterized by high-resolution TEM (HRTEM). The samples were prepared by E-beam evaporation of  $\text{SnO}_2$ /CNT onto carbon coated copper TEM grid, which was done at the same time as coating on interdigitated electrodes. A typical HRTEM image of CNT– $\text{SnO}_2$  composite is shown in Fig. 5e. From the HRTEM image, it can be identified that a single multi-walled CNT fragment is indeed embedded in the nanocrystalline  $\text{SnO}_2$  layer. The diameter of CNTs and the crystal size of  $\text{SnO}_2$  were estimated to be in the range of ~20–40 nm and 3–10 nm, respectively. Comparing to the TEM image of pure CNT (Fig. 2b), the nanotube walls cannot be resolved due to the presence of  $\text{SnO}_2$  nanocrystalline thin film surrounding the surface of CNT.

A plausible mechanism for CNT– $\text{SnO}_2$  co-evaporation can be drawn as follows. When  $\text{SnO}_2$  was evaporated at temperature of

~1500 °C in a vacuum of ~10<sup>-5</sup> Torr, CNTs fragments, which are small and very light, were carried into the vapor by surrounding  $\text{SnO}_2$  molecules. It should be noted that CNTs themselves were not decomposed during evaporation because this temperature is well below CNTs' sublimation point (>3000 °C) in a high vacuum condition. Thus, these results prove our new concept that CNTs can be co-evaporated with  $\text{SnO}_2$  material with no significant decomposition at the evaporation temperature of ~1500 °C. In addition, CNTs can endure treatment of high-energy electron beams (~7.67 kV) in a high vacuum of 10<sup>-5</sup> Torr. When CNT molecular fragments arrived at the substrate that was held at 130 °C,  $\text{SnO}_2$  vapor was condensed and coated around them. As the substrate was cooled down, CNTs remained in the lattice of  $\text{SnO}_2$  due to physicochemical binding between  $\text{SnO}_2$  and CNTs. This result is evident as seen in the TEM and SEM images. The fact that there should be physical binding between  $\text{SnO}_2$  and CNTs can also be inferred from other reports that demonstrate  $\text{SnO}_2$  coating around CNTs [9–14].

### 3.2. Sensor responses

The produced sensors were placed in a desiccator that served as a gas sensitivity test chamber. The total volume of the chamber is 22.35 l. Gas response (*S*) is calculated as follows:

$$S = \frac{R_{\text{gas}}}{R_{\text{air}}} \quad (5)$$

where  $R_{\text{air}}$  and  $R_{\text{gas}}$  are the resistances of the sensor in air and in the presence of desired gas, respectively.

The undoped  $\text{SnO}_2$  sensor, 0.5 wt% CNT– $\text{SnO}_2$  sensor and 1 wt% CNT– $\text{SnO}_2$  sensor show response to ethanol (EtOH) and methanol

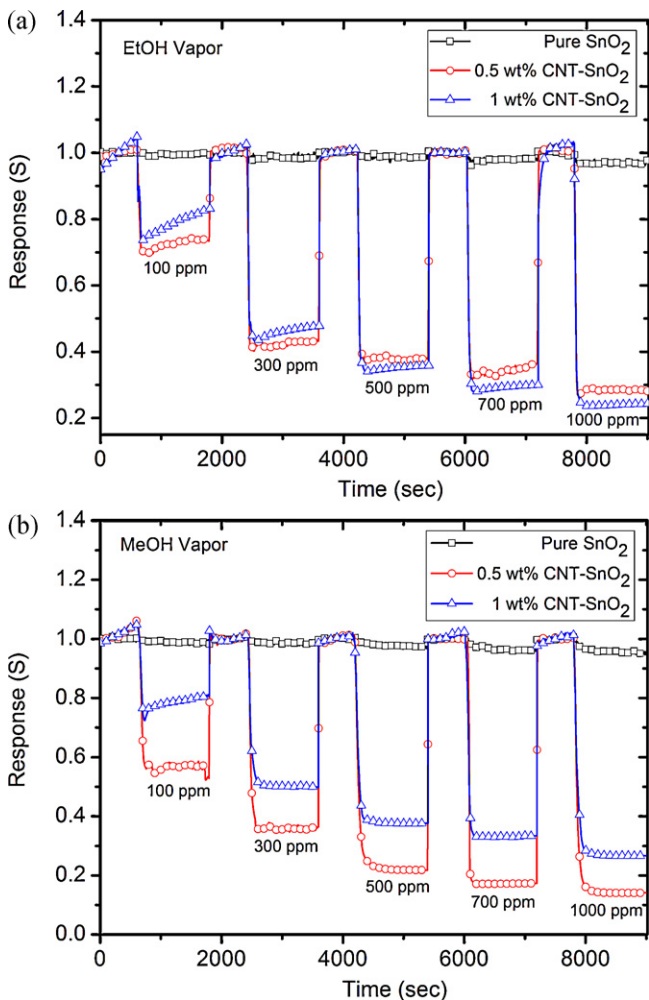


Fig. 6. Sensor responses of undoped  $\text{SnO}_2$  sensor, 0.5 wt% CNT– $\text{SnO}_2$  sensor and 1 wt% CNT– $\text{SnO}_2$  sensor to different concentrations of (a) EtOH and (b) MeOH.

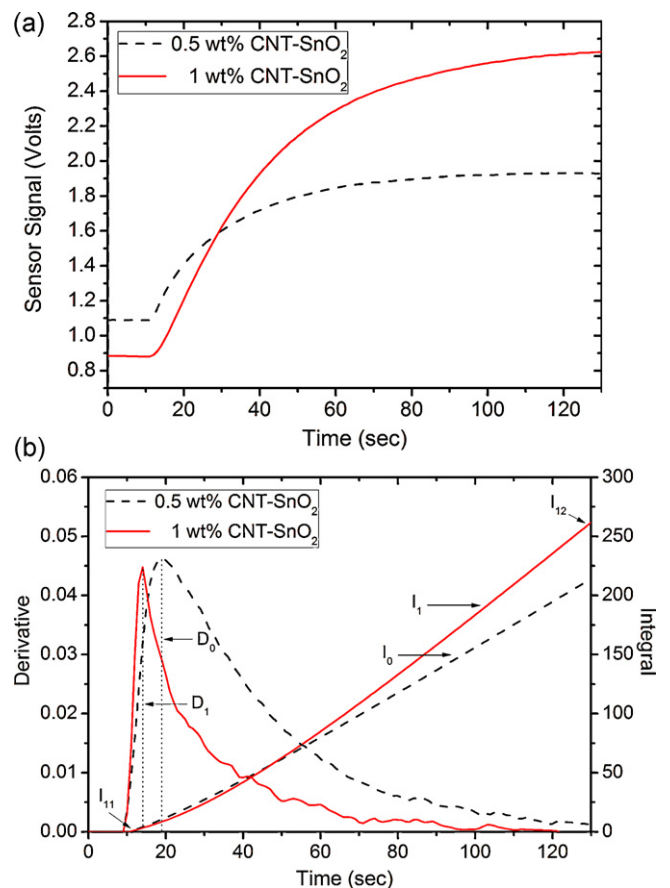


Fig. 7. (a) Raw responses (b) primary derivative and integral signals of gas sensors measured using portable E-nose.

(MeOH) as shown in Fig. 6a and b, respectively. It should be noted that the selected film thickness of 300 nm is an optimized value for electrical conductivity and sensitivity. It was found from our study that sensors with thickness of less than 200 nm and more than 400 nm will have too low and too high electrical conductivity, respectively. In addition, the gas-sensing response is increased as thickness increases from 50 nm to 200 nm and the response becomes quite independent of thickness as the thickness increases from 200 nm to 400 nm and begins to slowly decrease as the thickness increases further. In addition, a variation of less than 30% was found among ten tested sensors and the sensors have a long term drift of less than 20% over 6 months of operation. Thus, the fabricated sensors have reasonably good reproducibility and stability.

From Fig. 6, it can be seen that these materials behave as n-type semiconductors since their resistance decreases in the presence of a deoxidizing gas, whereas MWCNT–SnO<sub>2</sub> film prepared by spin-coating technique behave as p-type semiconductors [11]. Under the operating temperature range ~250–300 °C, CNT doping can improve the response of gas sensor on EtOH and MeOH compared with the pure SnO<sub>2</sub> sensor. The response of native SnO<sub>2</sub> sensor is lower than 2% while CNT-doped SnO<sub>2</sub> sensors give the response higher than 65% at concentration 1000 ppm under such temperature range. The amount of CNT doping exhibits different change in response to EtOH and MeOH vapors. Hence, the 0.5 wt% and 1 wt% of CNTs show highest response toward MeOH and EtOH, respectively. These results confirm that varying of CNT concentration can be used

to tune sensitivity and selectivity of SnO<sub>2</sub> sensor to a desired gas. In this case, the modified gas sensors can be employed to target MeOH vapor in the MeOH/EtOH mixture. Nevertheless, if CNT amount exceed, the gas sensitivity will be reduced because the CNTs begin to connect together and result in shorter resistance path [15].

### 3.3. Sensing mechanism of CNT–SnO<sub>2</sub> gas sensors

From the gas-sensing data, small percentage of CNT doping significantly enhances the sensing of MeOH and EtOH. The results are consistent with other reports based on CNT–SnO<sub>2</sub> composites [9–15]. In these reports, various explanations for gas-sensing enhancement by CNTs have been proposed, for examples, amplification effect of the PN junction structure between n-SnO<sub>2</sub> and p-SWCNT [9], the oriented growth of SnO<sub>2</sub> along the CNTs during heat treatment and its consequent enhancement of the local electric field favorable for the gas-sensing reaction [14] and increased surface area due to the formation of CNT protrusions [15]. The PN junction structure between SnO<sub>2</sub> and SWCNT is not applied in the present case because MWCNTs are used.

In this work, we propose that the observed enhancement effect is attributed to the nanochannels formed by MWCNTs embedded in SnO<sub>2</sub>. The formation of the nanochannels in SnO<sub>2</sub> surface can increase the diffusion of the gas molecules into the metal oxide surface as well as enhance local electric field at CNT–SnO<sub>2</sub> interface. This can considerably enhance dehydrogenation reactions of MeOH

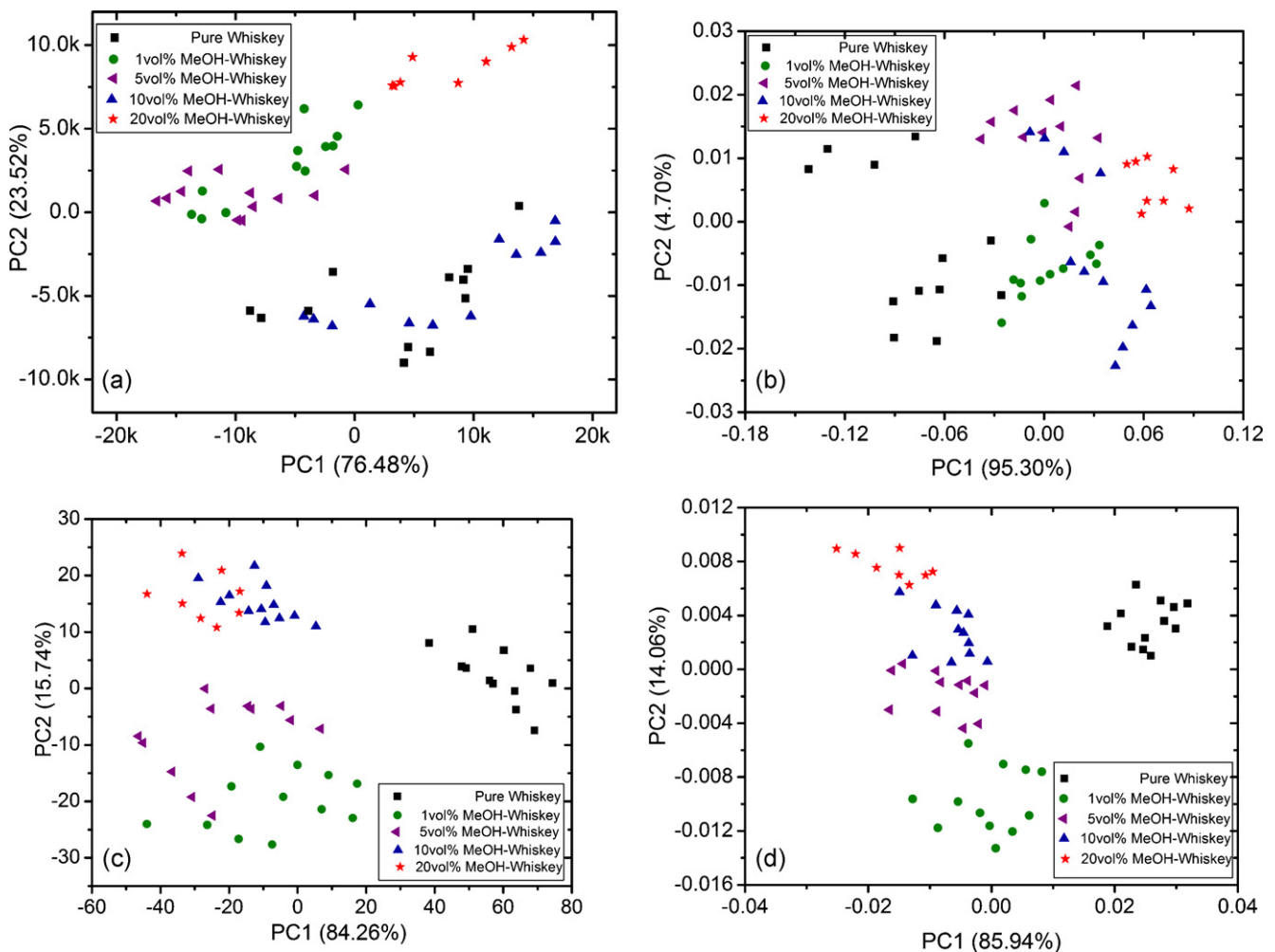
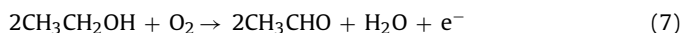
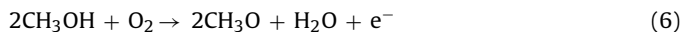


Fig. 8. PCA results using feature extraction from (a)  $\Delta R$ , (b)  $\Delta R/R_0$  and (c) integral and (d) primary derivative.

and EtOH as described by [23]:



Since the effect of CNTs on gas sensing is primarily on the surface, the gas-sensing response is not significantly dependent on the thickness when the thickness is sufficiently large. This is in accordance with our observations. Increasing surface area due to CNTs intrusion and observed smaller grain size due to CNTs doping can partly contribute to enhancing gas reaction. However, the contribution from these effects is relatively small because CNT concentration is so low that the specific surface area is only slightly affected by CNTs inclusion.

### 3.4. Electronic nose with PCA analysis

Since the fabricated sensors show different response to EtOH and MeOH, the E-nose based on such sensors can be applied to monitor MeOH contaminant in whiskey. Typical E-nose response to a whiskey is displayed in Fig. 7a while the integral and primary derivative of the response are shown in Fig. 7b. Because pure SnO<sub>2</sub> sensor gives a tiny response, the signal obtained from the pure SnO<sub>2</sub> sensor was neglected in further analysis.

From each sensor response curve, four different features were extracted for each sample. The first feature extraction is the conductance change, defined as  $\Delta R = R_{\text{gas}} - R_0$ . The second feature extraction is the relative response ( $\Delta R/R_0$ ). The third feature extraction is the integral. This feature was extracted by calculation of difference accumulative total reaction in the presence of sample gas, i.e.,  $I_{12} - I_{11}$  (see Fig. 7b). The last one is the primary derivative. The maximum amplitude in the same interval was employed, i.e.,  $D_0$  and  $D_1$  (see Fig. 7b). Each data set extracted from each proposed feature in the form of  $X_{56 \times 2}$  is introduced into the PCA process. PCA results of the data sets extracted by the proposed methods;  $\Delta R$ ,  $\Delta R/R_0$ , integral and primary derivative are shown in Fig. 8a–d, respectively.

The PCA results show that the feature extraction based on  $\Delta R$  cannot classify the contamination of MeOH in whiskey due to the drift effect of sensor signal depending on temperature variation in the long time measurement. The classical relative response ( $\Delta R/R_0$ ) seems to give a better result than  $\Delta R$  but many samples disperse in the same region and pure whiskey results locate rather close to whiskey having 1 vol% of MeOH contamination while MeOH content exceeding 2% (v/v) would harm the consumer [24]. In such case, the resolution power is not enough to guarantee the contamination of MeOH in whiskey. For feature extraction using both the integral and primary derivative data treatments, PCA results show a perfect classification between pure whiskey and whiskey having MeOH contamination. Moreover, the primary derivative can cluster all level of MeOH contaminations (1 vol%, 5 vol%, 10 vol% and 20 vol%) in the whiskey as shown in Fig. 8d. These results indicate that the proposed feature extractions, integral and primary derivative, provide good capabilities in the recognition and discrimination of MeOH contamination. These may be alternative ways to replace the common methods ( $\Delta R$  and  $\Delta R/R_0$ ) which are widely used in PCA analysis.

From our PCA results together with feature extraction technique, it can be seen that although the sensors are structurally similar, they can have sufficiently distinct response such that it can be used to discriminate different kind of similar odors. However, it should be noted that features extracted from response behaviors can be dependent on some measuring details such as chamber size, gas flow rate, and sensor position in the sensor chamber. Consequently, the feature extraction result can be considerably different for different E-nose systems. Nevertheless, it should not be a prob-

lem for E-nose applications because this can be well controlled for each E-nose system and any E-nose system must always be trained under a fixed condition.

## 4. Conclusions

We have reported the design, implementation and an example application of portable E-nose based on CNT–SnO<sub>2</sub> gas sensors including new feature extraction methods for improvement of data classification. The doping of CNTs could enhance the sensitivity of SnO<sub>2</sub> sensor while their concentration plays an important role in selectivity to volatile organic compounds such as EtOH and MeOH. The PCA results indicate that the newly proposed feature extraction including integral and primary derivative leads to higher classification performance as compared to the standard features ( $\Delta R$  and  $\Delta R/R_0$ ). The portable E-nose based on only two nanostructure sensors combined with proposed feature extraction methods shows clearly the classification of MeOH contamination mixed in the whiskey at higher concentrations than 1% by volume. It is hoped that such E-nose will be a useful tool for the whiskey industry and for quick screening of village-made whiskeys that are usually found of the MeOH contaminant.

## Acknowledgements

C.W. acknowledges the Commission on Higher Education for a Ph.D. scholarship under the program “Strategic Scholarships for Frontier Research Network”. T.K. expresses his great gratitude to the Thailand Research Fund (BRG5180023) for a research career development grant. Mahidol University and the National Science and Technology Agency are gratefully acknowledged for supports.

## References

- [1] M.P. Marti, R. Boque, O. Busto, J. Guasch, Electronic noses in the quality control of alcoholic beverages, *Trends Anal. Chem.* 24 (2005) 57–66.
- [2] H. Yu, J. Wang, Discrimination of Long Jing green-tea grade by electronic nose, *Sens. Actuators B, Chem.* 122 (2007) 134–140.
- [3] J.S. Vestergaard, M. Martens, P. Turkki, Application of an electronic nose system for prediction of sensory quality changes of a meat product (pizza topping) during storage, *LWT* 40 (2007) 1095–1101.
- [4] E. Scorsone, A.M. Pisanelli, K.C. Persaud, Development of an electronic nose for fire detection, *Sens. Actuators B, Chem.* 116 (2006) 55–61.
- [5] R.M. Negri, S. Reich, Identification of pollutant gases and its concentrations with a multisensor array, *Sens. Actuators B, Chem.* 75 (2001) 172–178.
- [6] A.C. Bastos, N. Magan, Soil volatile fingerprints: use for discrimination between soil types under different environmental conditions, *Sens. Actuators B, Chem.* 125 (2007) 556–562.
- [7] A.P.F. Turner, N. Magan, Electronic noses and disease diagnostics, *Nat. Rev. Microbiol.* 2 (2004) 161–166.
- [8] M. Pardo, G. Sberveglieri, Comparing the performance of different features in sensor arrays, *Sens. Actuators B, Chem.* 123 (2007) 437–443.
- [9] B.Y. Wei, M.C. Hsu, P.G. Su, H.M. Lin, R.J. Wu, H.J. Lai, A novel SnO<sub>2</sub> gas sensor doped with carbon nanotubes operating at room temperature, *Sens. Actuators B, Chem.* 101 (2004) 81–89.
- [10] E.H. Espinosa, R. Ionescu, B. Chambon, G. Bedis, E. Sotter, C. Bittencourt, A. Felten, J.J. Pireaux, X. Correig, E. Llobet, Hybrid metal oxide and multiwall carbon nanotube films for low temperature gas sensing, *Sens. Actuators B, Chem.* 127 (2007) 137–142.
- [11] N.V. Hieu, L.T.B. Thuya, N.D. Chien, Highly sensitive thin film NH<sub>3</sub> gas sensor operating at room temperature based on SnO<sub>2</sub>/MWCNTs composite, *Sens. Actuators B, Chem.* 129 (2008) 888–895.
- [12] J. Gong, J. Sun, Q. Chen, Micromachined sol-gel carbon nanotube/SnO<sub>2</sub> nanocomposite hydrogen sensor, *Sens. Actuators B, Chem.* 130 (2008) 829–835.
- [13] J. Wang, L. Liu, S.Y. Cong, J.Q. Qi, B.K. Xu, An enrichment method to detect low concentration formaldehyde, *Sens. Actuators B, Chem.* 134 (2008) 1010–1015.
- [14] J. Liu, Z. Guo, F. Meng, Y. Jia, J. Liu, A novel antimony-carbon nanotube-tin oxide thin film: carbon nanotubes as growth guider and energy buffer. Application for indoor air pollutants gas sensor, *J. Phys. Chem. C* 112 (2008) 6119–6125.
- [15] A. Wisitsoraat, A. Tuantranont, C. Thanachayanont, V. Patthanasettakul, P. Singjai, Electron beam evaporated carbon nanotube dispersed SnO<sub>2</sub> thin film gas sensor, *J. Electroceram.* 17 (2006) 45–49.
- [16] A. Wisitsoraat, A. Tuantranont, V. Patthanasettakul, T. Lomas, P. Chindaudom, Ion-assisted e-beam evaporated gas sensor for environmental monitoring, *Sci. Technol. Adv. Mater.* 6 (2005) 261–265.

- [17] H. Liu, G. Cheng, R. Zheng, Y. Zhao, C. Liang, Influence of synthesis process on preparation and properties of Ni/CNT catalyst, *Diamond Relat. Mater.* 15 (2006) 15–21.
- [18] T.C. Pearce, S.S. Schiffman, H.T. Nagle, J.W. Gardner, *Handbook of Machine Olfaction; Electronic Nose Technology*, Wiley-VCH, 2002.
- [19] C. Wongchoosuk, M. Lutz, T. Kerdcharoen, Correction of humidity effect for detection of human body odor, in: *Proceedings of the 5th ECTI-CON 2, 2008*, pp. 845–848.
- [20] I.T. Jolliffe, *Principal Component Analysis*, Springer, 2002.
- [21] S. Roussel, G. Forsberg, V. Steinmetz, P. Grenier, V. Bellon-Maurel, Optimisation of electronic nose measurement. Part I. Methodology of output feature selection, *J. Food Eng.* 37 (1998) 207–222.
- [22] S. Zhang, C. Xie, D. Zeng, Q. Zhang, H. Li, Z. Bi, A feature extraction method and a sampling system for fast recognition of flammable liquids with a portable E-nose, *Sens. Actuators B, Chem.* 124 (2007) 437–443.
- [23] S. Majumder, S. Hussain, S.N. Das, R.B. Bhar, A.K. Pal, Silicon doped SnO<sub>2</sub> films for liquid petroleum gas sensor, *Vacuum* 82 (2008) 760–770.
- [24] A.J. Paine, A.D. Dayan, Defining a tolerable concentration of methanol in alcoholic drinks, *Hum. Exp. Toxicol.* 20 (2001) 563–568.

## Biographies

**Chatchawal Wongchoosuk** received his B.Sc. with first class honors from Prince of Songkla University in 2005 and M.Sc. from Mahidol University in 2007 on Physics. At

present, he is a Ph.D. student at the Department of Physics, Mahidol University. His current research interests involve electronic noses, hybrid gas sensors and molecular simulation.

**Anurat Wisitsoraat** received his Ph.D., M.S. degrees from Vanderbilt University, TN, U.S.A., and B.Eng. degree in Electrical Engineering from Chulalongkorn University, Bangkok, Thailand in 2002, 1997, and 1993, respectively. His research interests include microelectronic fabrication, semiconductor devices, electronic and optical thin film coating, gas sensors, and micro-electromechanical systems (MEMS).

**Adisorn Tuantranont** is currently Lab director of Nanoelectronics and MEMS Laboratory, National Electronics and Computer Technology Center (NECTEC), under National Science and Technology Development Agency (NSTDA), Thailand. He received the B.S. degree from King Mongkut's Institute of Technology Ladkrabang (KMITL), Bangkok, Thailand in 1995, and the Ph.D. degree in 2001 from University of Colorado at Boulder, CO, USA, in Electrical Engineering. His current research interests are optical MEMS, microfluidic lab-on-a-chip and optoelectronics packaging.

**Teerakit Kerdcharoen** received B.Sc. and M.Sc. in Chemistry from Chulalongkorn University in 1990 and 1992, respectively. As an Exchange Student, he received his Ph.D. in Physical Chemistry from University of Innsbruck in 1995. Presently, he is a faculty member of Mahidol University. His research interests cover the topics of organic electronics ranging from theoretical modeling of materials to fabrication of devices such as tactile and chemical sensors.